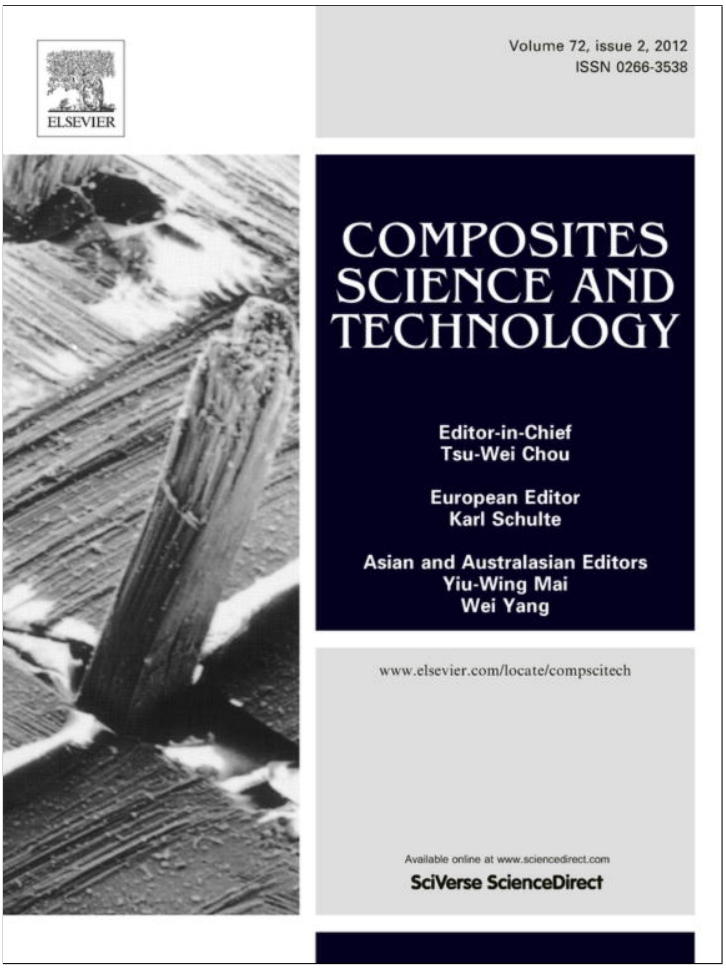

Composites Science and Technology 72 (2012) 175–181

Contents lists available at SciVerse ScienceDirect

Composites Science and Technology

journal homepage: www.elsevier.com/locate/compscitech

Relationship between wood elastic strain under bending and cellulose crystal strain

Cédric Montero [a,*], Bruno Clair [a], Tancrède Alméras [a], Arie van der Lee [b], Joseph Gril [a]

[a] Laboratoire de Mécanique et Génie Civil (LMGC), Université Montpellier 2, CNRS, France
[b] Institut Européen des Membranes (IEM), Université Montpellier 2, CNRS – UMR 5635, France

ARTICLE INFO

Article history:
Received 11 July 2011
Received in revised form 25 October 2011
Accepted 29 October 2011
Available online 6 November 2011

Keywords:
A. Wood
D. X-ray diffraction
B. Mechanical properties
C. Deformation
Cellulose
Micromechanics

ABSTRACT

Wood is a natural composite material with a complex multi-scale structure. Its stiffness is mainly due to crystalline cellulose fibrils reinforcing the cell walls. In order to quantify the contribution of cellulose to wood elastic properties in both tension and compression, the change in cellulose (004) lattice spacing (cellulose crystal strain) was measured by X-ray diffraction during a bending test on poplar specimens. A detailed methodology is presented to accurately quantify this cellulose crystal strain. Results show that during elastic loading, cellulose crystal strain is roughly proportional to wood strain. The strain ratio (cellulose crystal strain/wood strain) was close to 0.75, and did not differ significantly in tension and compression. Interpretation of the strain ratio with respect to cellulose orientation shows that part of the wood strain occurs without inducing cellulose crystal strain. This contribution amounts to 10–15% of wood strain, and its possible origin at different levels of wood ultra-structure is discussed.

1. Introduction

1.1. Wood as a composite material

Wood is one of the oldest and the most abundant natural composite material on earth. During hundred of millions years, it has been optimised by biological evolution to provide trees with their needs for mechanical support, leading to a very sophisticated structure with high mechanical performance [1]. Its use as a raw or transformed material is still increasing today in the context of growing concerns for environmental issues. Studying the origin of its mechanical properties basically aims at promoting and improving the use of this cheap and abundant resource. Since many principles of composite material design (cellular, multi-layered, fibre-reinforced, pre-stressed) exist in wood at different levels and are applied in an infinity of varieties depending on the tree species and the wood type, understanding the relationships between its ultra-structure at different length scales and its mechanical behaviour is also of fundamental interest for "bio-inspiration" [2].

1.2. Wood structure and properties

Wood is a cellular material made of multi-layered elongated cells (typically 1 mm long and 20 μm diameter). In between the cells, a middle lamella essentially made of lignins and pectins acts as a glue joint. The cell wall is divided into a primary wall and a secondary wall sub-divided in three layers (S1, S2, and S3). The material of which wall layers are made can be described as fibre-reinforced nanocomposite. Its fibre phase, made of partly crystalline cellulose microfibrils having nanometric width, is embedded in a matrix of lignin and hemicellulose. As the microfibrils represent an important fraction of the wall (approx. 50%) and have very high axial stiffness (more than 130 GPa), their organisation is determinant for the mechanical performance of the cell-wall. In each layer, cellulose microfibrils are generally not parallel to the cell axis, but organised as a helicoid around the cell oriented at a specific angle. The S2 layer is the more cellulosic and by far the thickest of the secondary layers, thus its microfibril angle (MFA) mainly governs the mechanical properties in the fibre direction [3]. A detailed description of wood multi-scale structure including graphical representation can be found in literature [4,5].

1.3. Wood micro-mechanics

Several models have been proposed to predict the mechanical properties of wood from the organisation and properties of cell wall components [5–8]. These models generally account for the cellular nature of wood, the composite nature of the cell wall and the effect of microfibril orientation. As wood cells have a very high aspect ratio, the behaviour of wood in its longitudinal direction is generally approximated as a parallel association of cell wall layers. Each cell wall layer is considered as a composite medium where microfibrils are also associated in parallel with the matrix phase. These assumptions implicitly consider infinitely long and

* Corresponding author. Tel.: +33 467149642; fax: +33 467143923.
E-mail address: cedric.montero@univ-montp2.fr (C. Montero).

0266-3538/$ - see front matter © 2011 Elsevier Ltd. All rights reserved.
doi:10.1016/j.compscitech.2011.10.014

straight fibres and/or microfibrils, and perfect cohesion between the components. In order to evaluate these assumptions, it is interesting to quantify the contribution of the individual components on the macroscopic behaviour. The behaviour of lignins and hemicelluloses was for a long time inaccessible from strain measurement until recent progress in spectroscopy tools made it possible to monitor strain of specific components [9]. Cellulose behaviour on the other hand is easier to measure thanks to its crystalline structure. Indeed, X-ray diffraction (XRD) patterns provide information about the orientation of cellulose in the cell wall (MFA) [10–12], but also about the state of strain of the cellulose crystal, through the analysis of changes in lattice spacing in response to mechanical loads [13,14].

1.4. XRD, crystal strain and micro-mechanics

XRD has been used in composite materials to quantify the respective contributions of the matrix and the reinforcing fibres to the apparent strain (e.g. [15]). A number of studies reported the strain of cellulose measured by XRD during mechanical tests performed on wood. Because cell-walls are fibre-reinforced composites, the axial strain of the microfibril is of particular interest. It can be observed through the change in position of the (004) reflection of the cellulose crystal. This method has been used to localise elastic strain during water sorption or desorption [14,16,17], to measure the crystal strain during internal stress release [16], and to monitor the change in mechanical stress during wood formation [18]. Experiments based on simple tensile tests [13,19–22] provide estimations of cellulose contribution to wood deformation. These studies revealed that the ratio between crystal strain and wood strain is always lower than 1, with a value generally ranging from 0.5 to 0.95. Only one study reports the behaviour of cellulose during compression tests [20], where the strain ratio ranged from 0.25 to 1.

The analysis of this ratio can bring useful information about the deformation process of a material at the ultra-structural scale. In the case of relatively simple composites, interpretation of these data can be rather straightforward in terms of strain localisation, because only one change in scale is involved between the crystal scale and the macroscopic scale (e.g. [15]). In the case of wood, however, many level of organisation are involved between the crystal (nanometre scale) and the macroscopic material (centimetre scale). Interpretation of the relation between crystal strains and wood strains can be given only under explicit assumptions about the mechanisms involved at each scale. For example, under the classical assumptions made in wood micro-mechanical models (infinitely long fibres and microfibrils, perfect cohesion between components and between layers) the strain ratio is expected to be related to the MFA by simple geometric considerations. Departure from this relation would indicate that some of the above-mentioned assumptions are not correct. Similarly, the strain ratio is expected to be the same under tensile and compressive loading, provided wood is loaded in its elastic domain.

1.5. Objectives

In order to check the real contribution of crystalline cellulose to wood elastic behaviour, a precise estimate of this strain ratio must be obtained on the same specimen both in tension and compression. This has been for the first time achieved here through the simultaneous observation of the two sides of a wood specimen submitted to a bending load. Here we present a four-point bending device designed for in situ XRD, allowing to measure with sufficient accuracy during a single test the behaviour of crystalline cellulose both under tension and compression. It aims at quantifying the contribution of cellulose to wood elastic strain and checking its linearity.

2. Material and method

2.1. Tested material

Experiments were performed on poplar (*Populus* spp.) wood (air-dry specific gravity approx. 0.55). Specimens were taken far enough from the pith to neglect ring curvature and machined at a size of $2 \times 3.2 \times 50$ mm^3 along radial, tangential and longitudinal direction (R, T, L) respectively. Experiments were performed in ambient conditions (22 ± 0.4 °C and 49 ± 7%RH). Specimens were taken in mature wood far enough from the pith to neglect ring curvature. Their orientation was chosen to get the direction of deflection parallel to the T direction and the X-ray beam perpendicular to the T direction, in order to minimise heterogeneity along strain profiles. The thickness along R was optimised to maximise the diffraction signal (trade-off between the amount of diffracting material and signal attenuation). The specimen height along T was set to maximise the measurement zone while keeping acceptable R/T ratio for bending tests.

2.2. Bending tests

Specimens were tested in four-point bending in joist orientation with 20 mm inner span and 40 mm outer span in a device specifically designed for the X-ray goniometer (Fig. 1). The screw-induced displacement of the inner holders applies pure bending on the specimen, inducing a linear strain gradient with compression on the upper side and tension on the lower side. Strain was recorded using two 5 mm-long strain gages (Kyowa KFG-5-120-C1-11-L1M3R) glued with cyanoacrylate adhesive at the mid-span of the specimen, on the tension and compression surfaces. Preliminary tests made on matched specimens showed that the linear elastic limits of the material were $\varepsilon^- = -0.22\%$ in compression and $\varepsilon^+ = 0.3\%$ in tension. Different strain levels (0.2%, 0.3%, 0.4%) were applied to the specimens in this experiment.

2.3. Experimental set-up for X-ray diffraction

Diffraction patterns were obtained with an X-ray diffractometer (Agilent Technologies Gemini S) using the Cu Kα source

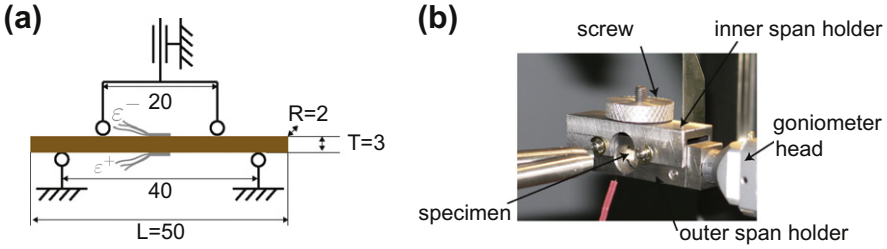

Fig. 1. (a) Schematic view of the four-point bending device and specimen dimensions (all dimensions in mm). ε^- and ε^+ are the strains measured with a strain gage on the upper (compressive) and lower (tensile) side, respectively. (b) Photography of four-point bending device specially designed for the X-ray goniometer head.

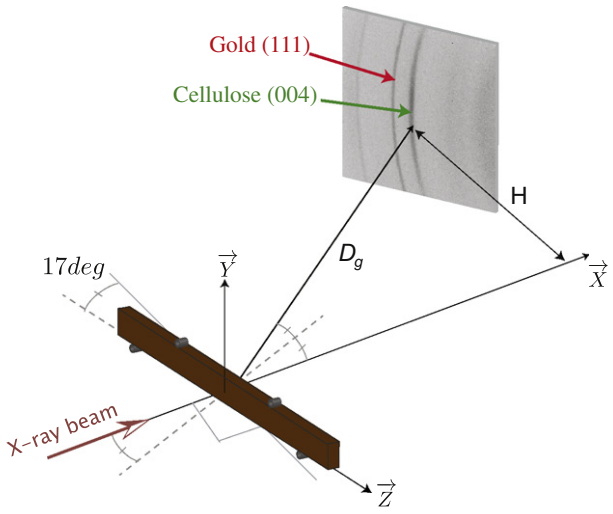

Fig. 2. Schematics of the experimental set-up for XRD in situ bending tests. The specimen is oriented at the Bragg angle (17°) from the normal to the X-ray beam position. D_g: distance between the outer surface of the specimen and the detector. H: distance between the centre of the transmitted beam and peak position of the diffraction peak.

(wavelength $\lambda = 0.154$ nm, operated at 50 kV and 30 mA) with a 0.8 mm collimator. The exposure time was set to 40 s to optimise the diffraction signal and the total test duration (approx. 30 min each profile). The detector was positioned at a distance $D = 135$ mm to the specimen, as to focus the signal acquisition on the first (004) reflection and maximise the resolution of the obtained data. The specimen was asymmetrically positioned according to the Bragg condition at 17° to maximise the intensity of the (004) reflection. The detector resolution was 2048 × 2048 pixels (31 μm/pixel) (Fig. 2).

The specimen was scanned from top to bottom both in the initial and deformed state with a step $\Delta y = 0.2$ mm. A diffraction pattern focused on the (004) plane was recorded at each step. The beam being fixed, the scan is performed by vertical translation of the bending device. The relative position y of the device is measured by a displacement sensor (Mitutoyo Absolute Digimatic Indicator) with 1 μm accuracy. Because the specimen is also translated during the bending, the position of the X-ray beam relative to the border of the specimen has to be precisely determined for each scan to compute a coherent strain field. This was done using a specific method based on the interpretation of the signal near the specimen border (see Appendix A). As a validation, the specimen height h is determined with this interpretation and compared to measurements made with the calliper. The specimen deflection after loading was also measured and found consistent with the measured strain under the assumptions of beam theory.

2.4. Determination of lattice spacing d_{004}

The cellulose crystal strain is measured by computing the displacement of the first reflection of the (004) crystal plane (which is normal to the cellulose microfibril axis). The theoretical (004) lattice spacing of cellulose is $d^{th}_{004} = 0.258$ nm, corresponding to a scattering angle of $2\theta^{th}_{004} = 34.73°$ for the considered wavelength. Slight changes in d_{004} due to mechanical strain induce a slight change in θ_{004} and therefore a displacement of the diffraction peak.

The lattice distance was calculated using Bragg's equation linking the wavelength of the X-ray source λ, to the lattice distance d_{004} and the scattering angle θ_{004}:

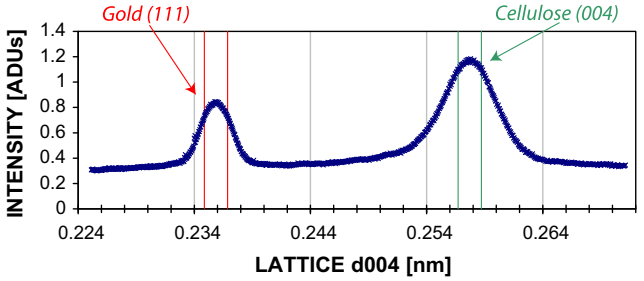

Fig. 3. Example of radial profile of cellulose (004) and gold (111) obtained from diffractogram integration.

$$\lambda = 2d_{004} \sin \theta_{004} \quad (1)$$

The exact scattering angle θ_{004} is obtained from its geometric relation with H_{004} (distance between the diffraction peak and beam centre measured on the detector), and D (distance between the specimen and the detector):

$$\tan \theta_{004} = H_{004}/D \quad (2)$$

In this analysis, the precision of the lattice spacing estimation critically depends on the precision obtained on these geometrical parameters. The relevant distance D to be taken into account is the distance between the detector and the centre of mass of the area of the specimen crossed by the beam. This distance must be calibrated each time a diffractogram is recorded, because the surface of the wood specimen is never perfectly plane and vertical and also because the wood specimen may slightly move out of plane during the experiment. For this purpose, a reference crystal material (spherical gold powder, particle size diameter: 0.5–0.8 μm, $d^{Au}_{111} = 0.235$ nm) was laid on the external surface of the specimen. The precise distance D_g between the specimen surface and the detector was determined from the position of the gold reflection. The distance D was defined as $D = D_g + R/2$ (with R the specimen width).

The azimuth distribution of the (200) cellulose reflection was used for the determination of the microfibril angle of the specimen using Cave's method [11]. The radial position of the (004) reflection was used to determine parameter H_{004}.

In these experimental conditions, the displacement of peak position H_{004} was only a few pixels. The following procedure was applied to get sub-pixel determination of this parameter: the diffractograms were integrated along the azimuth to obtain 1-D radial profiles between $2\theta = 33°$ and $2\theta = 40°$ (Fig. 3) and filtered to remove outlying data (Zinger spots due to cosmic radiation). The abscissa was converted into lattice spacing using Eqs. (1) and (2), and a second-order polynomial was fit to the data around the peak position. The precise position of the maximum, directly giving the lattice spacing d_{004}, was then computed from the polynomial coefficients.

2.5. Computation of strain profiles

The macroscopic strain field along specimen height h is assumed to be plane according to beam theory. Therefore the strain at any distance y from the upper surface of the specimen can be linearly interpolated from the gage measurements ε^+ and ε^-:

$$\varepsilon^{wood}(y) = \varepsilon^- - (\varepsilon^+ - \varepsilon^-)y/h \quad (3)$$

The profile of crystal strain $\varepsilon^{cryst}(y)$ is obtained from the estimations of the lattice spacing in initial and deformed states at position y:

$$\varepsilon^{cryst}(y) = d^{def}_{004}(y)/d^{ini}_{004}(y) - 1 \quad (4)$$

The occurrence of a small amount of stress relaxation during the test was minimised by the short duration of the test and neglected in further analyses.

3. Results

3.1. Profiles of lattice spacing and crystal strain

The recorded profiles of lattice spacing in initial and deformed states are shown in Fig. 4. Some variations of lattice spacing can be noticed along the initial profile. Variations near the border of the specimen are due to a weaker signal obtained at this level and other possible artefacts due to the state of wood near the surface and the presence of the strain gage. Data at these positions are removed in further analysis. Variations within the specimen are clearly observed but these sources of disturbance are independent of the applied stress so that they are also present in the deformed state, and will be eliminated when subtracting the lattice distances to obtain the strain.

The lattice profile in the deformed state clearly differs from that in initial state: the lattice distance is reduced on the upper part of the specimen corresponding to the compressed side, and increased on the lower part corresponding to the part under tension.

Cellulose crystal strain profiles computed from these data are shown in Fig. 5, together with the profile of macroscopic strain. The proximity between the middle of the specimen height and its neutral line (for which the strain is zero) confirms symmetrical specimen loading in tension and compression. The crystal strain is clearly negative in the upper part, positive on the lower part, and zero in the middle of the specimen. Although local variations can be noticed, the profile appears approximately linear. A comparison with the macroscopic strain shows that, at any position, the cellulose crystal strain is slightly lower in magnitude than the wood strain.

3.2. Cellulose lattice strain versus macroscopic strain

The relationship between wood macroscopic strain and cellulose crystal strain is shown in Fig. 6. This relationship is close to linear, showing that when wood is submitted to a strain, the cellulose deforms proportionally.

In order to detect a possible difference in response to compressive and tensile stresses, the average ratio Γ of crystal strain to wood strain was determined by linear regression independently for the compressed side ($\Gamma^- = 0.81$) and the tension side ($\Gamma^+ = 0.65$). A numerical difference was found for this specimen, and this experiment was repeated on different poplar specimens with similar MFA to check the significance of this result. Another example of result is shown in Fig. 7. The results of five tests (Table 1) show that the difference between the ratios obtained from the two sides is not significant.

Additional specimens were tested with larger strain up to the elastic limit of the material (see Table 1). Results for a same specimen at two strain levels are shown in Fig. 8. At higher strain levels, the results are similar to those shown in Figs. 4–6: the profile of crystal strain is linear along the specimen height, and its magni-

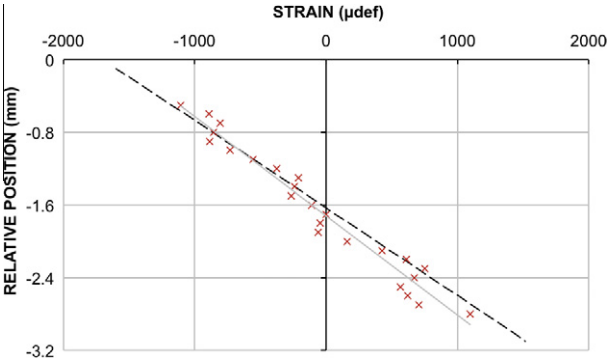

Fig. 5. Profile of cellulose crystal strain (×) and wood macroscopic strain (⌙ – –) along the height of specimen 1. The gray line (⌙——) indicates linear regression of the cellulose crystal strain.

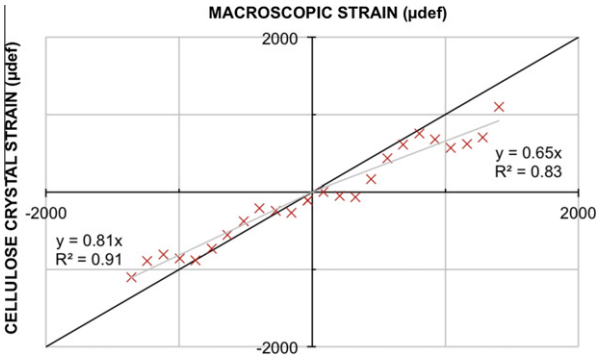

Fig. 6. Relationship between cellulose crystal strain and wood macroscopic strain (specimen 1). × Experimental results, ⌙—— linear regression of experimental results, ⌙ 1:1 line.

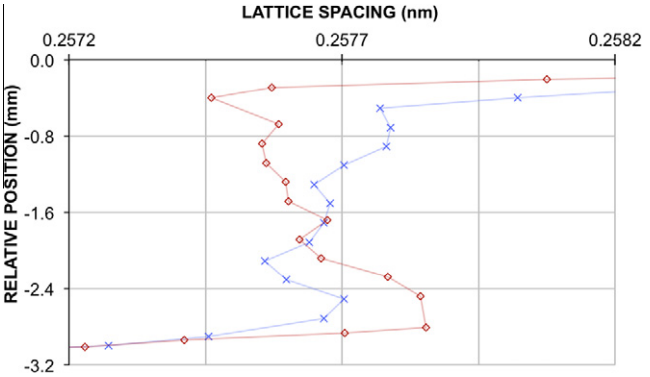

Fig. 4. Profiles of cellulose lattice spacing along the height of specimen 1, at the initial state (——×——) and deformed state (——◇——). The macroscopic strain applied is $\varepsilon^- = -0.194\%$ and $\varepsilon^+ = 0.184\%$.

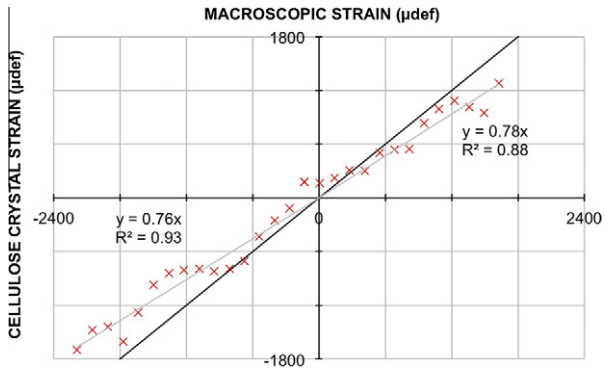

Fig. 7. Relationship between cellulose crystal strain and wood macroscopic strain (specimen 2) × experimental results, ⌙—— regression line of experimental results, ⌙ 1:1 line.

Table 1
Results of bending tests on different specimens. MFA: mean microfibril angle, $\Delta\varepsilon=(\varepsilon^{+}-\varepsilon^{-})/2$: macroscopic strain level applied, Γ^{-} (resp. Γ^{+}): mean strain ratio in the compressive zone (resp. tensile zone).

Specimen	MFA (°)	$\Delta\varepsilon$ (%)	Γ^{-}	Γ^{+}
1	17.7	0.1903	0.81	0.65
1*	17.7	0.3957	0.73	0.73
2	17.3	0.2175	0.76	0.78
3	18.0	0.2048	0.68	0.79
4	17.9	0.1975	0.71	0.76
MEAN$^{\pm sd}$	$17.7^{\pm 0.3}$	–	$0.738^{\pm 0.050}$	$0.742^{\pm 0.056}$

* Same specimen at two strain levels applied.

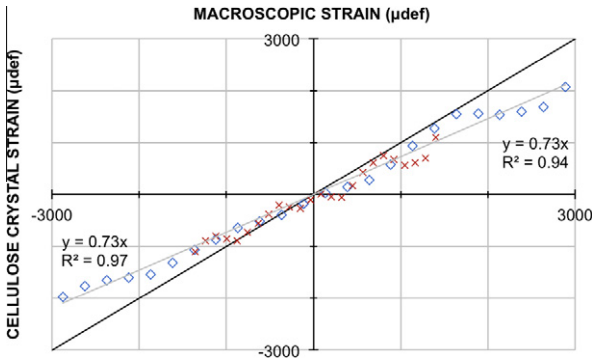

Fig. 8. Relationship between cellulose crystal strain and wood macroscopic strain (specimen 1) at two levels of applied strain; firstly at $\Delta\varepsilon = 0.1903\%$ (×) and secondly increased at $\Delta\varepsilon = 0.3957\%$ (◇). The grey lines (——) indicate linear regressions on data relative to the larger strain level.

tude is proportional to that of wood strain, both on the compression and on the tension sides. The obtained Γ ratios were close to those obtained at a strain of 0.2% (Table 1).

4. Discussion

4.1. Measuring lattice strain

Our results show that the strain of crystalline cellulose can be measured with sufficient precision to evaluate its contribution to macroscopic wood strain. It is noted that the profile of cellulose apparent lattice spacing is often found non-uniform inside the unloaded wood specimen. This heterogeneity of lattice spacing at the initial state is due to at least two factors: (1) a possible artefact due to heterogeneity of specimen density. Indeed, heterogeneity (*e.g.* due to the presence of the large cavities of vessels) induces slight changes in the position of the centre of mass of the specimen. Error propagation analysis shows that an error of 100 μm in the estimation of the position of centre of mass induces an error of 0.00014 nm on the estimation of lattice spacing (equivalent to a strain of 0.05%). (2) The presence of eigenstresses in the material (*e.g.* due to heterogeneous drying shrinkage of the specimen), leading to a heterogeneous state of cellulose strain prior to loading. In order to cope with this heterogeneity, it is necessary to carefully monitor the position of each exposition, in order to compute crystal strain by subtracting the lattice spacing measured on the same material points before and after loading. To do so, we designed a specific procedure based on the interpretation of the signal at the specimen border (see Appendix A) and calibration with gold powder.

4.2. Linearity of cellulose strain

We tested wood specimens up to their proportional stress/strain limit, and checked that, within this range, cellulose strain is proportional to macroscopic strain. This proportionality was checked in three ways: comparing different positions corresponding to different strain levels within the bent specimen; comparing the tensile and compressed sides of the specimen; comparing the strain ratio obtained for different applied strain levels.

Our conclusions are in accordance with most in situ tensile tests performed at low strain levels [13,19–21]. However, in contrast with earlier reports [20], we show that the strain ratio does not differ significantly in tension and compression. This was made possible by the use of a bending test, where the specimen is symmetrically loaded in tension and compression at the same time. Coincidence of the neutral line between wood strain and cellulose crystal strain confirms that they are proportional within the specimen, suggesting that any possible localised effects due to *e.g.* the compression at the loading points are of second-order.

4.3. Micro-mechanical interpretation of strain ratio

The strain ratio we obtained is nearly 0.75, which is in the range of values reported in tensile tests: Suzuki [13] estimated a ratio of 0.65, and Nakai et al. [21] reported a ratio between 0.55 and 0.85. Only Peura et al. [22] reports a much lower ratio (approx. 0.1), but this was obtained on very thin specimens for which the estimated specific modulus of elasticity was also unusually low.

Interpretation of this strain ratio involves at first order the geometrical effect of the MFA. Indeed, cellulose microfibrils are not aligned with the fibre axis, so that the strain in the direction of cellulose ε^{C} is related to the strain in the principal directions of the fibre wall through the microfibril angle μ. The rigorous formula for this relation is: $\varepsilon^{C} = c^2\varepsilon_L^W + s^2\varepsilon_T^W - cs\varepsilon_S^W$, where $s = \sin\mu$, $c = \cos\mu$, ε_L^W and ε_T^W are the strains in the longitudinal and transverse directions of the cell wall, respectively, and ε_S^W is the shear strain in the wall. Because the wood is loaded only in its longitudinal direction parallel to the cell wall axis, the transverse stress in the cell wall is neglected, so that the strain of the cell wall is related to the longitudinal strain through the Poisson's ratio (ν_{LT}^W) of the wall: $\varepsilon_T^W = -\varepsilon_L^W\nu_{LT}^W$. Following a number of authors [8,23,24], we assume that shear strains are fully restrained at the cell-wall level $(\varepsilon_S^W = 0)$, because they are prevented by the cohesion and anti-parallel configuration of adjacent cell walls. Under this assumption, the relationship between cellulose strain and wall longitudinal strain reduces to:

$$\varepsilon^{C} = \varepsilon_L^W(c^2 - s^2\nu_{LT}^W) \tag{5}$$

Note that, for the strain level considered in this experiment, the change in the MFA due to the deformation of the specimen is negligible (it can be easily shown from geometrical consideration and was experimentally demonstrated by Peura et al. [22]), so that a unique value of μ can be used. The Poisson's ratio of the cell wall can be estimated from micro-mechanical models [24]. For the MFA used in our experiment ($\mu = 17°$), the model estimates $\nu_{LT}^W \approx 0.8$, so that the estimation of the ratio $\varepsilon^{C}/\varepsilon_L^W$ is 0.85. This quantitative estimation of the effect of MFA shows that it is not sufficient to explain the observed values of strain ratio. Nakai et al. [21] report strain ratios estimated from tensile tests on specimens with different MFA, ranging from 0.3 (MFA = 21°) to 0.95 (MFA = 9°). Our calculations show that, for that set of observation too, the effect of the MFA was not sufficient to explain the observed values.

The difference between experimental estimates of strain ratio and those expected from the geometrical effect of the MFA can be ascribed to other deformation mechanisms occurring in wood. The effect of amorphous cellulose associated in series with the crystalline material has been recognised as a possible factor by previous authors [21,22]. Indeed, this mechanism is able to generate

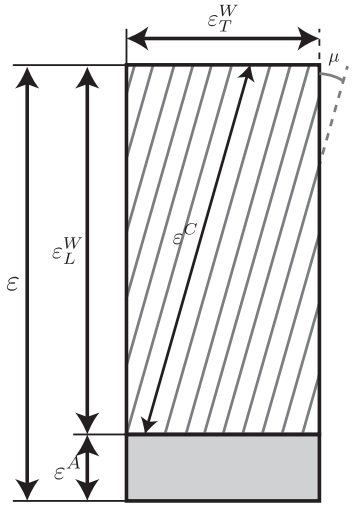

Fig. 9. Schematic representation of the sources of longitudinal deformation in wood. Total strain ε can be divided into a contribution from the cell-wall ε_L^W, that depend on the crystal strain ε^C through the MFA μ, and an additive contribution ε^A that does not involve the deformation of crystalline material.

macroscopic strain without generating crystal strain, and could therefore partly explain why the strain ratio is lower than expected from purely geometrical considerations. This effect can be represented by an additive contribution ε^A to the total strain, independent of the crystal strain ε^C, as illustrated in Fig. 9.

The relation between total strain, crystal strain, MFA and this additive contribution is expressed by:

$$\varepsilon = \varepsilon^C/(c^2 - s^2\nu_{LT}^W) + \varepsilon^A \quad (6)$$

Actually, due to the complex hierarchical structure of wood, many alternative mechanisms may contribute to macroscopic strain without contributing to crystal strain. (i) At the macroscopic level, an effect of grain angle, a slight difference between the direction of wood fibres and the longitudinal direction of the specimen, would induce a projection effect similar to that of the MFA. (ii) At a sub-millimetric scale, wood is not only made of fibres but also of a small fraction of different types of cells called ray parenchyma, oriented in the radial direction of wood, i.e. perpendicular to fibres. The loading of wood along the fibre direction probably generates complex strain fields near the areas where rays are present, possibly involving bending and shear effects that would contribute to ε^A. (iii) The wood fibre itself is actually hollow and tapered, so that some bending of the wall is also likely to happen and have a similar effect. (iv) Wood fibres are glued together by an amorphous component called the middle lamella. At that level, wood can be considered as a fibre-reinforced composite where the matrix is the middle lamella and the reinforcing elements are wood fibres. In such composites, stress redistribution induces a so-called "shear-lag" effect, resulting in strain concentrations near the fibre ends and therefore smaller strain in the fibres fraction than in the bulk material, as has been shown on artificial composites (e.g. [15]). (v) At the level of the cell-wall, we here assumed a full shear restraint, following previous authors [23], but the occurrence of a small amount of shear has been considered by other authors and cannot be ruled out without further verification. Such an effect would indeed also contribute to decreasing the microfibril strain/wall strain ratio. (vi) Moreover, the fibre wall itself has a multilayer structure, and shear strain could possibly occur at the interface between layers, so that the strain at the level of a given layer could also be lower than the strain of the bulk wall. (vii) Each layer is constituted of cellulose microfibrils reinforcing a matrix of lignin and hemicelluloses. The cellulose microfibrils are neither perfectly straight nor infinitely long. As a consequence, a slight initial curvature of the microfibrils could result in bending effects that would partly allow the extension of the wall material without extending the microfibril itself. (viii) Finally, the finite length of the microfibrils induces a shear lag effect, which may also contribute to explain the difference between crystal strain and wall strain.

In order to discriminate between these mechanisms or evaluate their relative contribution, complementary observations at the relevant length scales would be necessary. Our experiment however provides an estimation of their cumulated effect through the estimation of ε^A. The total contribution of these "additive" effects due to localised shear, bending deformations or extension of amorphous material is evaluated (using Eq. (6)) near 12% of the total strain for the poplar wood we studied. This can be considered as a second-order effect regarding elastic strain, justifying why most models of elastic properties neglect these factors and concentrate on the effect of cell-wall layered structure and microfibril orientation. However, the behaviour of these amorphous compartments may be of primary importance regarding wood hygroscopic behaviour (see e.g. [17]), and possibly other non-elastic wood behaviour, such as visco-elastic creep, mechanosorptive creep or post-elastic response.

5. Conclusion

A methodology was developed to precisely evaluate the crystal strain of cellulose during a bending test. Results show that during elastic deformations, cellulose crystal strain remains proportional to wood macroscopic strain. The mean strain ratio measured on four specimens was close to 0.75 and did not differ significantly between tension and compression. The effect of cellulose orientation was taken into account through classical projection formula. This analysis showed that the values of strain ratio can be only partly explained by this geometrical effect, and evidenced a contribution of strains located in non-crystalline components of wood. This contribution was evaluated to be approximately 12% of macroscopic strains, and hypotheses for its origin are proposed.

Acknowledgements

The authors would like to thanks Mr. Gilles Camp (LMGC) for the realisation of the bending apparatus. This work has been performed in the framework of the "MechWood" project supported by the Austrian Research Promotion Agency (FFG, 815234/12791) and regularly discussed during meetings of European COST Action FP0802 "Experimental and Computational Micro-Characterization Techniques in Wood Mechanics".

Appendix A

Measurements of lattice strain are performed by subtracting the lattice spacing recorded in deformed and initial state. Because the state of cellulose is substantially heterogeneous within a piece of wood, it is critical to record lattice spacing before and after loading *at the same position* within the specimen. For this, the displacement induced by the bending must be precisely accounted for. We designed a specific procedure to do so.

The principle of this procedure is to use variations in signal intensity occurring near the specimen border (Fig. A1a) to locate the relative position y_C of the beam centre. Let R_b be the beam radius and Δy the distance between successive shoots (with $\Delta y < 2R_b$, so that successive shoots overlap, see Fig. A1b). We assume that the signal intensity is, at first order, proportional to the amount of crystalline cellulose crossed by the beam, i.e. to the area of wood S illuminated by the beam (Fig. A1c). When a

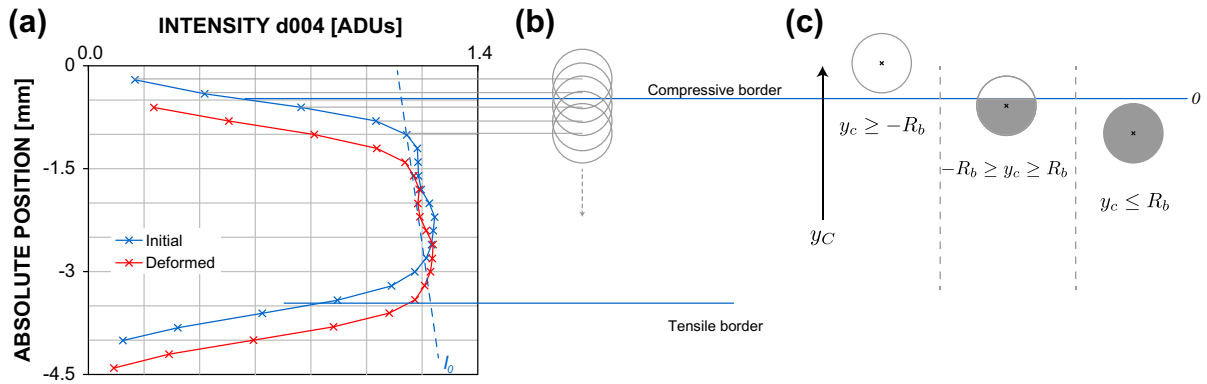

Fig. A1. (a) Profiles of signal intensity along specimen height y, at initial and deformed states. (b) Beam overlap for successive shoots and (c) relationship between beam centre position and diffracting wood area.

shoot is made outside of the specimen ($y_C > R_b$) the diffracting wood area is zero ($S = 0$). When the shoot is entirely within the specimen ($y_C < -R_b$), the diffracting wood area constant ($S = S_0 = \pi R_b^2$). In between, the diffracting area is directly related to the distance y_C between the beam centre and the specimen border:

$$S(y_C) = 2\int_0^{y_C+R_b} (R_b^2 - (y - y_C)^2)^{1/2}\,dy \text{ for } -R_b \leqslant y_C \leqslant R_b \qquad (S1)$$

The intensity for full diffraction I_0 corresponding to an illuminated wood area S_0 can be estimated from the data in the core of the specimen. Then, the illuminated area S for any shoot can be estimated from the corresponding intensity I: $S = I * S_0/I_0$. By solving Eq. (S1) numerically, the value of y_C can be deduced from the value of S.

Finally, the position to be associated to a given shoot is the centre of mass of the diffracting area, y_G. It can be deduced from y_C using Eq. (S2):

$$y_G = f(y_c) = \frac{2}{S(y_c)}\int_0^{y_c+R_b} y(R_b^2 - (y - y_c)^2)^{1/2}\,dy \qquad (S2)$$

This procedure is based on the assumption that the amount of crystalline material (and therefore diffraction intensity) is uniform within the sample. Fig. A1a shows that this is only approximately true within the core of the sample. The procedure happens nevertheless to be quite robust to this assumption, since the height of the specimens determined with this method was very close to that determined with a calliper (relative difference ≈1%). Moreover, variations in signal intensity are highly reproducible (as attested by comparison of the two curves of Fig. A1a), so that if this heterogeneity induces a slight error on the determined position, the same error will be made on the two profiles, so that the calculation of strain will refer to the same material points and remains valid.

References

[1] Salmén L, Burgert I. Cell wall features with regard to mechanical performance. A review COST action E35 2004 – 2008: wood machining – micromechanics and fracture. Holzforschung 2009;63:121–9.
[2] Martone PT, Boller M, Burgert I, Dumais J, Edwards J, Mach K, et al. Mechanics without muscle: biomechanical Inspiration from the Plant World. Integr Compar Biol 2010;50:888–907.
[3] Cave ID. The anisotropic elasticity of the plant cell wall. Wood Sci Technol 1968;2:268–78.
[4] Eitelberger J, Hofstetter K. Prediction of transport properties of wood below the fiber saturation point – a multiscale homogenization approach and its experimental validation Part I: thermal conductivity. Compos Sci Technol 2011;71:134–44.
[5] Salmén L. Micromechanical understanding of the cell-wall structure? Comptes Rendus Biol 2004;327:873–80.
[6] Salmén L. A model for the prediction of fiber elasticity. Wood Fiber Sci 1985;17:336–50.
[7] Harrington JJ, Booker R, Astley RJ. Modelling the elastic properties of softwood – Part I: the cell-wall lamellae. Holz Als Roh-und Werkstoff 1998;56:37–41.
[8] Hofstetter K, Hellmich C, Eberhardsteiner J. Micromechanical modeling of solid-type and plate-type deformation patterns within softwood materials. A review and an improved approach. Holzforschung 2007;61:343–51.
[9] Åkerholm M, Salmén L. Interactions between wood polymers studied by dynamic FT-IR spectroscopy. Polymer 2001;42:963–9.
[10] Yamamoto H, Okuyama T, Yoshida M. Method of determining the mean microfibril angle of wood over a wide-range by the improved cave's method. Mokuzai Gakkaishi 1993;39:375–81.
[11] Cave ID. Theory of X-ray measurement of microfibril angle in wood. Forest Prod J 1966;16:37–42.
[12] Ogurreck M, Müller M. Analytical description of the scattering of cellulose nanocrystals in tracheid wood cells. J Appl Crystallogr 2010;43:256–63.
[13] Suzuki M. Mechanical deformation of crystal lattice of cellulose in Hinoki wood. Mokuzai Gakkaishi 1968;14:268–75.
[14] Sobue N, Shibata Y, Mizusawa T. X-Ray measurement of lattice strain of cellulose crystals during the shrinkage of wood in the longitudinal direction. Mokuzai Gakkaishi 1992;38:336–41.
[15] Young RJ, Eichhorn SJ, Shyng YT, Riekel C, Davies RJ. Analysis of stress transfer in two-phase polymer systems using synchrotron microfocus X-ray diffraction. Macromolecules 2004;37:9503–9.
[16] Clair B, Alméras T, Yamamoto H, Okuyama T, Sugiyama J. Mechanical behavior of cellulose microfibrils in tension wood, in relation with maturation stress generation. Biophys J 2006;91:1128–35.
[17] Zabler S, Paris O, Burgert I, Fratzl P. Moisture changes in the plant cell wall force cellulose crystallites to deform. J Struct Biol 2010;171:133–41.
[18] Clair B, Alméras T, Pilate G, Jullien D, Sugiyama J, Riekel C. Maturation stress generation in poplar tension wood studied by synchrotron radiation microdiffraction. Plant Physiol 2011;155:562–70.
[19] Suzuki M. Relation between Young's modulus and the cell wall structures of Sugi (Cryptomeria japonica D. Don). Mokuzai Gakkaishi 1969;15:268–75.
[20] Nakai T, Yamamoto H, Nakao T. The relationship between macroscopic strain and crystal lattice strain in wood under uniaxial stress in the fiber direction. J Wood Sci 2005;51:193–4.
[21] Nakai T, Yamamoto H, Nakao T, Hamatake M. Mechanical behavior of the crystal lattice of natural cellulose in wood under repeated uniaxial tension stress in the fiber direction. Wood Sci Technol 2006;40:683–95.
[22] Peura M, Kölln K, Grotkopp I, Saranpää P, Müller M, Serimaa R. The effect of axial strain on crystalline cellulose in Norway spruce. Wood Sci Technol 2007;41:565–83.
[23] Schniewind AP, Barrett JD. Wood as a linear orthotropic viscoelastic material. Wood Sci Technol 1972;6:43–57.
[24] Alméras T, Gril J, Yamamoto H. Modelling anisotropic maturation strains in wood in relation to fibre boundary conditions, microstructure and maturation kinetics. Holzforschung 2005;59:347–53.